IEEE Access
Multidisciplinary | Rapid Review | Open Access Journal

Received 5 January 2023, accepted 13 January 2023, date of publication 16 January 2023, date of current version 23 January 2023.

*Digital Object Identifier 10.1109/ACCESS.2023.3237565*

RESEARCH ARTICLE

# Intelligent Attitude Fault-Tolerant Control of Space Tumbling Target Fly-Around Based on RBF Neural Network

**SHUANG LIANG AND YASHENG ZHANG**
Space Engineering University, Beijing 101416, China
Corresponding author: Shuang Liang (shuangshuangsmart@163.com)

**ABSTRACT** The flying around monitoring task of space tumbling target is one of the key links of its on-orbit service. Considering the practical constraints of system inertia uncertainty, external disturbance, actuator saturation, and fault in engineering practice, a robust composite controller based on radial basis function (RBF) neural network is proposed. First, in a new line of sight rotation (RLOS) coordinate system, the relative attitude kinematics and dynamics equations between the tracker and tumbling target based on the error quaternion are established; second, the RBF neural network is used to estimate the additive and multiplicative faults of the system, and the fast nonsingular terminal sliding mode surface (FNTSMS) is combined with the active disturbance rejection control (ADRC) technology to design a finite-time fault-tolerant control (FTC) strategy with high accuracy, strong robustness, and anti-saturation based on the RBF neural network. It is proven that the designed robust fault-tolerant controller can ensure that the system state error converges to a small region containing the origin in a limited time under the Lyapunov framework. Finally, the effectiveness and superiority of the control strategy were verified by numerical simulation.

**INDEX TERMS** Space tumbling target, FTC, attitude error quaternion, RBF neural network, ADRC, FNTSMS.

## I. INTRODUCTION

As of February 4, 2022, according to the statistical data of the U.S. space surveillance network, there were 25182 space targets, including 8171 spacecraft and 17011 rocket bodies and debris [1]. Most space debris in the vast space, due to the influence of gravity and perturbation, gradually evolved into rolling motion states such as rotation, precession, and nutation, becoming the main pollution source of the space environment and posing a great threat to the development and safety of the aerospace industry. Therefore, the development of on-orbit maintenance, fuel refueling, capture, and recovery tasks for space debris is of great significance for extending the life of spacecraft, removing space debris, improving on-orbit service capabilities, and maintaining the safety and stability of the space environment [2], [3], [4], [5]. The relative motion control of space tumbling targets, such as flying around, rendezvous, docking, and tracking, is one of the key technologies for completing the above tasks. In recent decades, an increasing number of countries and institutions have committed to this work. Although spacecraft has been strictly and thoroughly tested before entering space, it is always in a space environment of electromagnetic interference, space gravity, and uncertain interference during its mission life, which poses a great threat and challenge to the long-term effective operation of spacecraft, and many spacecraft will fail [6], [7], [8], [9], [10]. Therefore, in order to ensure the safe and successful completion of space missions, FTC methods should be studied to ensure the stability and reliability of spacecraft. Generally, it is divided into two categories: passive FTC and active FTC. Spacecraft FTC methods have increasingly become one of the research hotspots.

At present, many effective techniques and methods for spacecraft attitude active fault tolerance have been proposed, such as sliding mode control, adaptive control, control assignment, and composite controller. Moreover, since the concept

The associate editor coordinating the review of this manuscript and approving it for publication was Junhua Li.

of specific performance was proposed in the literature [11], the research on attitude FTC technology gradually presents a trend, that is, it is not limited to the pursuit of good steady-state and transient performance, but more inclined to study the comprehensive control problems with multiple specific performances. For example, in [12], [13], and [14], terminal sliding mode control and output feedback control scheme based on H∞ observer are respectively used to solve the attitude maneuver control problem in the case of an actuator failure, internal uncertainty, and external disturbance. On basis of considering the specific performance above, reference [15] achieved limited convergence performance by designing an adaptive fuzzy second-order terminal sliding mode control scheme. References [16], [17] also considered the installation error and dislocation of the actuator and flywheel and designed more complex control strategies to achieve stable tracking. In addition, for more complex control objects, a fault-tolerant attitude-tracking control scheme for flexible spacecraft was designed [18], and the active fault-tolerant attitude-tracking control of a single cabin spacecraft model with a moving center of mass was implemented [19]. Through the discussion of the above researches, the control methods, and other specific performance of spacecraft attitude FTC problems have been relatively mature, but most of the researches still focus on the space targets with strong cooperation and stable attitude.

As a special kind of space target, the control problems of space tumbling targets, such as synchronous flying around, approaching, tracking, rendezvous, and docking, have become a hot research topic in the field of on-orbit service. For example, in [20], [21], [22], [23], and [24], considering external interference, configuration uncertainty, actuator constraints, and other practical problems, effective adaptive control, sliding mode control, and other control schemes are designed to achieve space rolling target tracking, approach, hovering position tracking, and attitude synchronization. However, these studies did not consider actuator failures and losses. At present, there are relatively few studies on the FTC of the close relative motion of space tumbling targets. In [25], under the condition of unknown model parameters, external interference, actuator saturation, and failure, the control problem of rendezvous and docking between autonomous robot and space rolling target is studied based on sliding mode control technology and adaptive method. A robust fault-tolerant controller combining sliding mode control and adaptive technology was proposed by Hu et al. to solve the close-range operation of spacecraft and free-floating rolling objects under practical problems such as unexpected interference, the uncertainty of the mass inertial characteristics of the tracking device, and actuator failure [26]. In [27], by designing two fixed time position controllers, the timing FTC of spacecraft rendezvous and docking with a free-rolling target in the presence of external interference and propeller failure was studied. The above research on the FTC of space tumbling targets are all modeled in line-of-sight coordinate systems or body coordinate systems, but traditional modeling methods have certain limitations for special research objects such as space tumbling targets [28]. References [22], [29], [30], [31] proposed a new concept of the RLOS coordinate system and verified the effectiveness of the RLOS coordinate system by designing reasonable control schemes. On this basis, this paper will continue to carry out the research on the attitude of FTC of space tumbling target fly-around. In addition, there have been many mature research results on spacecraft attitude, such as SO (3) [32], quaternion [33], Rodriguez [34], etc. In this study, the error quaternion attitude dynamics equations will be established in the RLOS coordinate system.

The observer, RBF neural network, adaptive control, and other methods have been used to deal with system faults, unknown models, and disturbances in many existing types of research. A nonsingular TSMC based on RBF neural network is proposed by Sun et al. [35] to solve the problem of predetermined time trajectory tracking for uncertain manipulator systems. RBF neural network is used to estimate unknown dynamic functions, and the stability time can be adjusted as a controller parameter. In [36], a terminal sliding mode observer (SMO) that can make all state estimation errors converge to zero in a finite time is proposed. On this basis, a fault reconstruction method based on the concept of equivalent output error injection and a fault isolation strategy based on SMO are proposed, and the effectiveness of fault reconstruction is proved by the simulation of a small unmanned underwater vehicle. Reference [37] also used SMO to reconstruct actuator faults and disturbances in a limited time. In [38], aiming at the problem of system state and actuator fault deviation estimation of Lipschitz nonlinear systems, a new descriptor SMO is proposed to accurately estimate the equipment state and actuator fault deviation. Based on this estimation, an integral sliding mode control scheme is proposed, and a developed stability criterion is established. The extended observer is used to estimate the total uncertainty in [17]. In [39], a secure model-free adaptive controller with a completely unknown dynamic model is designed by using the compact dynamic linearization method. Reference [40] designed a dynamic estimator with tradeoff state information to solve the problem of the unpredictable real state of the system in the design of an adaptive feedback control scheme.

Motivated by the aforementioned observations and methods, this paper focuses on the finite-time FTC scheme for space tumbling target fly-around under the conditions of external interference, internal modeling uncertainty, actuator performance failure, and saturation constraints. The main contributions of this paper can be summarized in the following two aspects:

(1) Aiming at the attitude FTC problem of space tumbling target fly-around, a relative attitude motion model is established based on a new coordinate system. Based on the traditional LOS coordinate system, the rotation of the line-of-sight itself is considered, which directly

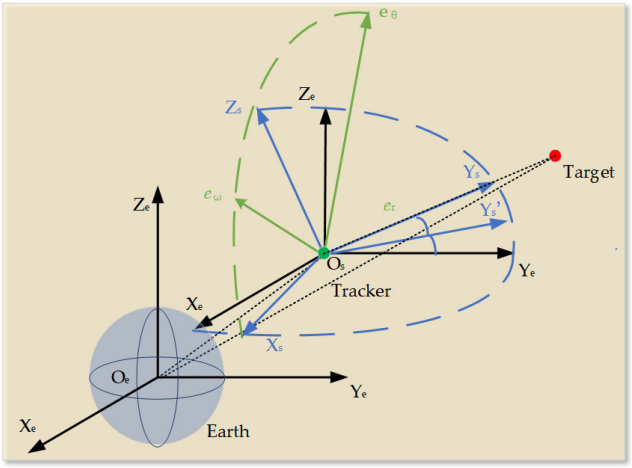


**FIGURE 1.** Relative motion coordinate system.

reflects the relative motion characteristics of non-cooperative targets.

(2) In order to further clarify the cause and value of uncertainty in engineering practice, this paper adopts a composite control strategy based on RBF neural network. The nonlinear function fitting ability of the RBF neural network is used to estimate and compensate for the nonlinear part caused by multiplication and addition faults of the actuator online, and the ESO in the composite controller is used to estimate the nonlinear part caused by external interference and internal uncertainty. The effectiveness and superiority of the results are verified through the comparison of simulation experiments.

## II. RELATIVE MOTION MODEL

### A. RELATIVE MOTION CONTROL BASED ON THE LVLH COORDINATE SYSTEM

The coordinate system is shown in Figure 1. The J2000 geocentric inertial coordinate system $O_e - X_eY_eZ_e$ is defined as that the coordinate origin is geocentric $O_e$, the direction of axis $O_eX_e$ is from the geocentric to J2000 equinox, the direction of axis $O_eZ_e$ is the normal vector direction of the epoch plane equatorial plane, and the axis $O_eY_e$ is determined by the right-hand rule. The line-of-sight (LOS) coordinate system $O_s - X_sY_sZ_s$ is defined as the coordinate origin $O_s$ at the centroid of the tracker, the axis $O_sY_s$ points to the target centroid along the line of sight, the axis $O_sZ_s$ is vertical to the axis $O_sY_s$ in the vertical plane, and the axis $O_sX_s$ is determined by the right-hand rule. The rotating line-of- sight (RLOS) coordinate system $O_s - e_re_\theta e_\omega$ is defined as the coordinate origin $O_s$ at the centroid of the tracker, $\boldsymbol{e}_r$ is the unit vector along the line of sight direction, $\boldsymbol{e}_\omega$ is the unit vector along the line of sight angular velocity direction, and the unit vector $\boldsymbol{e}_\theta$ meets the right-hand coordinate system [28]. The coordinate system of the tracker body $O_s - X_bY_bZ_b$ is defined as the coordinate origin $O_s$ at the centroid of the tracker, and the $O_sX_b$, $O_sY_b$, and $O_sZ_b$ axes are connected to the spacecraft along the inertia axis of the tracker.

### B. RELATIVE ATTITUDE MOTION EQUATION

According to Euler's theorem, the transformation between the coordinate systems can be achieved by rotating the Euler angle. In order to avoid singularity, this study uses a quaternion to describe the attitude motion of spacecraft, because there may be a large angle maneuver when the tracker flies around the tumbling target. The tracker attitude quaternion $\boldsymbol{q}$ is defined as the quaternion of J2000 geocentric inertial coordinate rotating to the current body coordinate system of the tracker; The expected attitude quaternion $\boldsymbol{q}_d$ is defined as the quaternion of J2000 geocentric inertial coordinate system rotating to the desired body coordinate system of the tracker; The error quaternion $\boldsymbol{q}_e$ is defined as the quaternion of the desired body coordinate system when the tracking spacecraft rotates from the current body coordinate system. In this study, the expected body coordinate system of the tracker is the RLOS coordinate system.

The expression of error quaternion [29] is:

$$\boldsymbol{q}_e = \boldsymbol{q}_d^{-1} \otimes \boldsymbol{q} = \begin{bmatrix} q_{d0} & \bar{\boldsymbol{q}}_d^T \\ -\bar{\boldsymbol{q}}_d & q_{d0}\boldsymbol{I}_{3\times3} - \tilde{\bar{\boldsymbol{q}}}_d \end{bmatrix} \otimes \boldsymbol{q} \tag{1}$$

where $\otimes$ is the quaternion operation symbol; $q_{d0}$ and $\bar{\boldsymbol{q}}_d = \begin{bmatrix} q_{d1} & q_{d2} & q_{d3} \end{bmatrix}^T$ are the scalar and vector parts of $\boldsymbol{q}_d$ respectively; and $\tilde{\bar{\boldsymbol{q}}}_d$ is the antisymmetric matrix of $\bar{\boldsymbol{q}}_d$.

The expression of tracker attitude quaternion is:

$$\dot{\boldsymbol{q}} = \frac{1}{2}\begin{bmatrix} -\boldsymbol{q}^T & q_0\boldsymbol{I}_{3\times3} + \tilde{\bar{\boldsymbol{q}}} \end{bmatrix}\boldsymbol{\omega} \tag{2}$$

where, $q_0$ and $\bar{\boldsymbol{q}} = \begin{bmatrix} q_1 & q_2 & q_3 \end{bmatrix}^T$ are the scalar and vector parts of $\boldsymbol{q}$ respectively, and $\tilde{\bar{\boldsymbol{q}}}$ is the antisymmetric matrix of $\bar{\boldsymbol{q}}$, $\boldsymbol{\omega} = \begin{bmatrix} \omega_x & \omega_y & \omega_z \end{bmatrix}^T$ is the angular velocity vector of the tracker.

The expression of tracker expected attitude quaternion is:

$$\dot{\boldsymbol{q}}_d = \frac{1}{2}\begin{bmatrix} -\boldsymbol{q}_d^T & q_{d0}\boldsymbol{I}_{3\times3} + \tilde{\bar{\boldsymbol{q}}}_d \end{bmatrix}\omega_d \tag{3}$$

where, $\boldsymbol{\omega}_d = \begin{bmatrix} \omega_{dx} & \omega_{dy} & \omega_{dz} \end{bmatrix}^T$ is the desired attitude angular velocity vector.

By combining Eq. (1), (2), and (3), the error angular velocity vector can be expressed as:

$$\boldsymbol{\omega}_e = \boldsymbol{\omega} - \boldsymbol{A}(\boldsymbol{q}_e)\boldsymbol{\omega}_d \tag{4}$$

where, $\boldsymbol{A}(\boldsymbol{q}_e) = \left(q_{e0}^2 - \bar{\boldsymbol{q}}_e^T\bar{\boldsymbol{q}}_e\right)\boldsymbol{I}_{3\times3} + 2\bar{\boldsymbol{q}}_e^T\bar{\boldsymbol{q}}_e - 2q_{e0}\tilde{\bar{\boldsymbol{q}}}_e$, $\boldsymbol{\omega}_e = \begin{bmatrix} \omega_{xe} & \omega_{ye} & \omega_{ze} \end{bmatrix}^T$, $\boldsymbol{A}(\boldsymbol{q}_e)$ meets $\left\|\boldsymbol{A}(\boldsymbol{q}_e)\right\| = 1$, and $\dot{\boldsymbol{A}}(\boldsymbol{q}_e) = -\tilde{\boldsymbol{\omega}}_e\boldsymbol{A}(\boldsymbol{q}_e)$. $q_{e0}$ and $\bar{\boldsymbol{q}}_e = \begin{bmatrix} q_{e1} & q_{e2} & q_{e3} \end{bmatrix}^T$ are the scalar and vector components of $\boldsymbol{q}_e$, respectively.

The relative motion equation of the attitude based on the error quaternion description can be obtained as follows:

$$\dot{\boldsymbol{q}}_e = \frac{1}{2}\begin{bmatrix} 0 & -\boldsymbol{\omega}_e^T \\ \boldsymbol{\omega}_e & -\tilde{\boldsymbol{\omega}}_e \end{bmatrix}\boldsymbol{q}_e \tag{5}$$

### C. RELATIVE ATTITUDE DYNAMICS EQUATION

According to the theorem of the momentum moment of a rigid body, the attitude dynamics equation based on the Euler angle is:

$$\boldsymbol{J}\dot{\boldsymbol{\omega}} = -\tilde{\boldsymbol{\omega}}\boldsymbol{J}\boldsymbol{\omega} + \boldsymbol{u} \tag{6}$$

where $\boldsymbol{J} = \boldsymbol{J}^T = \text{diag}(\begin{bmatrix} I_x & I_y & I_z \end{bmatrix})$ denotes the inertia tensor, $\boldsymbol{u}$ denotes the actual control torque, and $\tilde{\boldsymbol{\omega}}$ denotes the anti-symmetric matrix of $\boldsymbol{\omega}$.

Considering the input saturation of the actuator, the actual control torque $\boldsymbol{u}$ is expressed as

$$\boldsymbol{u} = \text{sat}(\boldsymbol{u}_c) = \begin{cases} \boldsymbol{u}_{\max}, & \boldsymbol{u}_c \geq \boldsymbol{u}_{\max} \\ \boldsymbol{u}_c, & |\boldsymbol{u}_c| < \boldsymbol{u}_{\max} \\ -\boldsymbol{u}_{\max}, & \boldsymbol{u}_c \leq -\boldsymbol{u}_{\max} \end{cases} \tag{7}$$

where $\boldsymbol{u}_c$ is the ideal control law, $\boldsymbol{u}_{\max}$ is the saturation value of control torque, the result of deviation between the above two equations is:

$$\Delta\boldsymbol{u} = \boldsymbol{u} - \boldsymbol{u}_c \tag{8}$$

Considering the actuator failure, the expression [41] is

$$\begin{cases} \boldsymbol{u}_c = \boldsymbol{\Gamma}\boldsymbol{\tau}_c + \bar{\boldsymbol{\tau}}_c \\ \boldsymbol{\Gamma} = \boldsymbol{\Gamma}_0 + \Delta\boldsymbol{\Gamma} \end{cases} \tag{9}$$

where $\boldsymbol{\tau}_c$ is the output control command, $\bar{\boldsymbol{\tau}}_c$ is the additive failure error, $\boldsymbol{\Gamma} = \text{diag}(\rho_1, \ldots, \rho_n) \in \mathbb{R}^{n\times n}$ indicates the control efficiency, $0 \leq \rho_i \leq 1$ indicates the working state of the $i$th actuator, and $\boldsymbol{\Gamma}_0$ is the nominal value. Regardless of $\boldsymbol{\Gamma}$ changes, it is positive-definite.

Considering the uncertainty of moment of inertia, the expression is:

$$\boldsymbol{J} = \boldsymbol{J}_0 + \Delta\boldsymbol{J} \tag{10}$$

where $\boldsymbol{J}_0$ and $\Delta\boldsymbol{J}$ denote the nominal and uncertain parts of the moment of inertia, respectively.

Based on the above Eq. (6), (7), (8), (9), and (10), considering the uncertainty of moment of inertia, external disturbance, actuator failure and saturation constraints, the attitude dynamics equation of the tracker is:

$$\begin{aligned}(\boldsymbol{J}_0 + \Delta\boldsymbol{J})\dot{\boldsymbol{\omega}} = (\boldsymbol{\Gamma}_0 + \Delta\boldsymbol{\Gamma})\boldsymbol{\tau}_c - \tilde{\boldsymbol{\omega}}(\boldsymbol{J}_0 + \Delta\boldsymbol{J})\boldsymbol{\omega} \\ + \bar{\boldsymbol{\tau}}_c + \Delta\boldsymbol{u} + \boldsymbol{w}\end{aligned} \tag{11}$$

where, $\boldsymbol{w}$ is external disturbance.

The derivative of Eq. (4) is as follows

$$\begin{aligned}\dot{\boldsymbol{\omega}}_e &= \dot{\boldsymbol{\omega}} - \dot{A}(\boldsymbol{q}_e)\dot{\boldsymbol{\omega}}_d + \tilde{\boldsymbol{\omega}}_e\boldsymbol{A}(\boldsymbol{q}_e)\boldsymbol{\omega}_d \\ &= (\boldsymbol{J}_0 + \Delta\boldsymbol{J})^{-1}[(\boldsymbol{\Gamma}_0 + \Delta\boldsymbol{\Gamma})\boldsymbol{\tau}_c - \tilde{\boldsymbol{\omega}}(\boldsymbol{J}_0 + \Delta\boldsymbol{J})\boldsymbol{\omega} \\ &\quad + \bar{\boldsymbol{\tau}}_c + \Delta\boldsymbol{u} + \boldsymbol{w}] - \boldsymbol{A}(\boldsymbol{q}_e)\dot{\boldsymbol{\omega}}_d + \tilde{\boldsymbol{\omega}}_e\boldsymbol{A}(\boldsymbol{q}_e)\boldsymbol{\omega}_d \\ &= (\boldsymbol{J}_0 + \Delta\boldsymbol{J})^{-1}[(\boldsymbol{\Gamma}_0 + \Delta\boldsymbol{\Gamma})\boldsymbol{\tau}_c + \bar{\boldsymbol{\tau}}_c + \Delta\boldsymbol{u} + \boldsymbol{w}] + \boldsymbol{h}_e\end{aligned} \tag{12}$$

where, $\boldsymbol{h}_e = (\boldsymbol{J}_0 + \Delta\boldsymbol{J})^{-1}[-\tilde{\boldsymbol{\omega}}(\boldsymbol{J}_0 + \Delta\boldsymbol{J})\boldsymbol{\omega}] - A\left(\boldsymbol{q}_e\right)\dot{\boldsymbol{\omega}}_d + \tilde{\boldsymbol{\omega}}_e A\left(\boldsymbol{q}_e\right)\boldsymbol{\omega}_d$.

The following formula can be obtained from both sides of Eq. (5):

$$\begin{aligned}\ddot{\boldsymbol{q}}_e = &\frac{1}{2}\begin{bmatrix} 0 & -\boldsymbol{h}_e^T \\ \boldsymbol{h}_e & -\tilde{\boldsymbol{h}}_e \end{bmatrix}\boldsymbol{q}_e + \frac{1}{2}\begin{bmatrix} 0 & -\boldsymbol{\omega}_e^T \\ \boldsymbol{\omega}_e & -\tilde{\boldsymbol{\omega}}_e \end{bmatrix}\dot{\boldsymbol{q}}_e \\ &+ \frac{1}{2}\begin{bmatrix} -\boldsymbol{q}_e^T \\ q_{e0}\boldsymbol{I}_{3\times3} + \tilde{\tilde{\boldsymbol{q}}}_e \end{bmatrix}(\boldsymbol{J}_0 + \Delta\boldsymbol{J})^{-1} \\ &\times (\Gamma\boldsymbol{\tau}_c + \bar{\boldsymbol{\tau}}_c + \Delta\boldsymbol{u} + \boldsymbol{w})\end{aligned} \tag{13}$$

According to literature [42], $(\boldsymbol{J}_0 + \Delta\boldsymbol{J})^{-1} = \boldsymbol{J}_0^{-1} + \Delta\tilde{\boldsymbol{J}}$, $\Delta\tilde{\boldsymbol{J}} = -\boldsymbol{J}_0^{-1}\Delta\boldsymbol{J}(I_3 + \boldsymbol{J}_0^{-1}\Delta\boldsymbol{J})^{-1}\boldsymbol{J}_0^{-1}$. Then, $\boldsymbol{h}_e = \boldsymbol{h}_{e0} + \Delta\boldsymbol{h}_e$, $\boldsymbol{h}_{e0} = -\boldsymbol{J}_0^{-1}\tilde{\boldsymbol{\omega}}\boldsymbol{J}_0\boldsymbol{\omega} - A\left(\boldsymbol{q}_e\right)\dot{\boldsymbol{\omega}}_d + \tilde{\boldsymbol{\omega}}_e A\left(\boldsymbol{q}_e\right)\boldsymbol{\omega}_d$, $\Delta\boldsymbol{h}_e = \boldsymbol{J}_0^{-1}(-\tilde{\boldsymbol{\omega}}\Delta\boldsymbol{J}\boldsymbol{\omega}) + \Delta\tilde{\boldsymbol{J}}[-\tilde{\boldsymbol{\omega}}(\boldsymbol{J}_0 + \Delta\boldsymbol{J})\boldsymbol{\omega}]$.

The relative motion attitude dynamics equation based on the error quaternion is summarized as follows:

$$\ddot{\boldsymbol{q}}_e = \boldsymbol{F} + \boldsymbol{f}_0 + \boldsymbol{C}_1 + \boldsymbol{C}_2 + \boldsymbol{C}_0\boldsymbol{\tau}_c \tag{14}$$

where,

$$\boldsymbol{F} = \frac{1}{2}\begin{bmatrix} 0 & -\Delta\boldsymbol{h}_e^T \\ \Delta\boldsymbol{h}_e & -\Delta\tilde{\boldsymbol{h}}_e \end{bmatrix}\boldsymbol{q}_e + \frac{1}{2}\begin{bmatrix} -\boldsymbol{q}_e^T \\ q_{e0}\boldsymbol{I}_{3\times3} + \tilde{\tilde{\boldsymbol{q}}}_e \end{bmatrix}(\boldsymbol{J} + \Delta\boldsymbol{J})^{-1}\boldsymbol{w},$$

$$\boldsymbol{f}_0 = \frac{1}{2}\begin{bmatrix} 0 & -\boldsymbol{\omega}_e^T \\ \boldsymbol{\omega}_e & -\tilde{\boldsymbol{\omega}}_e \end{bmatrix}\dot{\boldsymbol{q}}_e + \frac{1}{2}\begin{bmatrix} 0 & -\boldsymbol{h}_{e0}^T \\ \boldsymbol{h}_{e0} & -\tilde{\boldsymbol{h}}_{e0} \end{bmatrix}\boldsymbol{q}_e,$$

$$\boldsymbol{C}_0 = \frac{1}{2}\begin{bmatrix} -\boldsymbol{q}_e^T \\ q_{e0}\boldsymbol{I}_{3\times3} + \tilde{\tilde{\boldsymbol{q}}}_e \end{bmatrix}\boldsymbol{J}_0^{-1}\Gamma_0,$$

$$\boldsymbol{C}_1 = \frac{1}{2}\begin{bmatrix} -\boldsymbol{q}_e^T \\ q_{e0}\boldsymbol{I}_{3\times3} + \tilde{\tilde{\boldsymbol{q}}}_e \end{bmatrix}(\boldsymbol{J}_0^{-1} + \Delta\tilde{\boldsymbol{J}})(\Delta\boldsymbol{u} + \bar{\tau}_c),$$

$$\boldsymbol{C}_2 = \frac{1}{2}\begin{bmatrix} -\boldsymbol{q}_e^T \\ q_{e0}\boldsymbol{I}_{3\times3} + \tilde{\tilde{\boldsymbol{q}}}_e \end{bmatrix}(\Delta\tilde{\boldsymbol{J}}\Gamma + \boldsymbol{J}_0^{-1}\Delta\Gamma)\tau_c.$$

### D. CONTROL PROBLEM DESCRIPTION

Some practical problems will be faced when flying around space tumbling targets. To further design the controller and facilitate simulation verification, the following reasonable assumptions are made:

*Assumption 1:* External disturbance $\boldsymbol{w}$ is unknown and bounded, and the boundary $\bar{\boldsymbol{w}}$ is an unknown constant, there is $\|\boldsymbol{w}\| \leq \bar{\boldsymbol{w}}$.

*Assumption 2:* The uncertain part of the moment of inertia $\Delta\boldsymbol{J}$ is unknown and bounded, and the boundary $\Delta\bar{\boldsymbol{J}}$ is an unknown constant, there is $\|\Delta\boldsymbol{J}\| \leq \Delta\bar{\boldsymbol{J}}$.

*Assumption 3:* The additive failure error $\bar{\boldsymbol{\tau}}_c$ is unknown and bounded.

*Assumption 4:* Since the output of the actuator has a maximum value, $\Delta\boldsymbol{u}$ is unknown and bounded, and the boundary $\Delta\bar{\boldsymbol{u}}$ is an unknown constant, there is $\|\Delta\boldsymbol{u}\| \leq \Delta\bar{\boldsymbol{u}}$.

*Assumption 5:* The tumbling target to be studied is a regular precession target, its precession angle ($\psi$) rate and spin angle ($\varphi$) rate are constant; the nutation angle ($\theta$) rate is 0.

*Assumption 6:* In a classical fly-around scene, the tracker follows the spin axis of the tumbling target; that is, the fly-around the form of the IRPL [28] parallels the spin axis of the tumbling target in the relative motion model in this study.

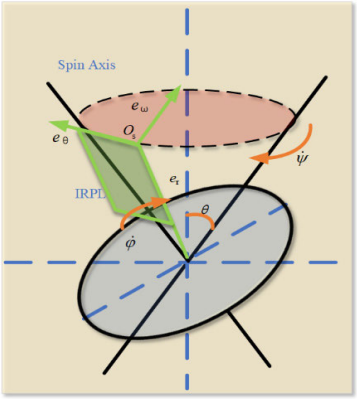


**FIGURE 2.** Schematic diagram of synchronous flight around.

Therefore, the desired attitude coordinate system $O_s - e_r e_\theta e_\omega$ is shown in Figure 2.

Description of control objectives: aiming at the problem of flying around attitude control of space tumbling targets in the presence of moment of inertia uncertainty, external interference, actuator failure, and saturation, a finite-time controller with anti-saturation, interference suppression, and FTC with strong anti-interference ability and robustness is designed based on the attitude dynamics equation of error quaternion, meeting assumptions 1 to 4.

*Remark 1:* The error attitude dynamics model Eq. (14) established in this study is based on the line-of-sight rotation coordinate system, a new coordinate system for studying the relative motion of the space tumbling target proposed in [22], [29], [30], and [31]. On this basis, this paper further studies its disturbance suppression and attitude fault tolerance problems.

## III. DESIGN AND STABILITY ANALYSIS OF THE COM-POUND CONTROLLER

The main idea of controller design in this study is to use FNTSMS nonlinear state error feedback form on the basis of the traditional ADRC, and to estimate uncertain parameters by combining RBF neural network and ESO.

### A. PSO-RBF NEURAL NETWORK

An RBF neural network can approximate any nonlinear function with high accuracy. Compared with BP neural network model and traditional physical model, RBF neural network has stronger approximation ability, classification ability and learning speed, and is simple in structure and easy to train, with good applicability. Therefore, based on RBF network model, this paper approaches the unknown part of the model [43].

The RBF neural network model is composed of three layers. $\boldsymbol{X} = [x_1, x_2, \ldots, x_m]^{\mathrm{T}}$ is the m-dimensional vector of the input layer. $\boldsymbol{Y} = [y_1, y_2, \ldots, y_p]^{\mathrm{T}}$ is the p-dimensional vector of the output layer, which is a simple linear function. $\boldsymbol{H} = [h_1, h_2, \ldots, h_n]^{\mathrm{T}}$ is the hidden layer, which is composed of radial action functions. $\boldsymbol{W} = [w_{11}, w_{12}, \ldots, w_{1\mathrm{p}}; \ldots; w_{\mathrm{n}1}, w_{\mathrm{n}2}, \ldots, w_{\mathrm{np}}]$ is the weight from the hidden layer to the output layer. The hidden layer generally takes the Gaussian function, which can be expressed as follows:

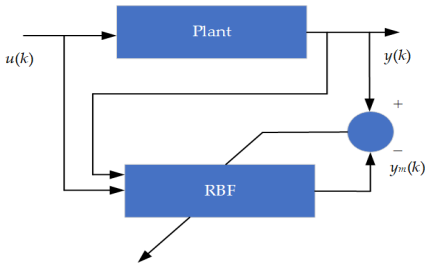


**FIGURE 3.** RBF neural network estimator.

$$h_i(x) = \exp\left[-\frac{(x - \boldsymbol{G}_i)^{\mathrm{T}}(x - \boldsymbol{G}_i)}{2b_i^2}\right] \quad (i = 1, 2, \ldots, n) \tag{15}$$

where, $h_i$ is the output of the $i$th hidden node; $\boldsymbol{B} = [b_1, b_2, \ldots, b_i]^{\mathrm{T}}$ is the normalized constant vector, representing the width; $\boldsymbol{G}_i = [g_{1i}, g_{2i}, \ldots, g_{mi}]^{\mathrm{T}}$ is the central vector of the Gaussian basis function.

The output layer functions are as follows:

$$y_j = \sum_{k=1}^{n} w_{kj} h_k \quad (j = 1, 2, \ldots, p) \tag{16}$$

This study mainly uses RBF neural network with 7-10-4 structure to two uncertain parameters in the nonlinear system model: the actuator deviation faults $\boldsymbol{C}_1$ and actuator gain faults coefficient $\boldsymbol{C}_2$. The input layer vectors of the two RBF neural networks are both $\boldsymbol{X} = [\boldsymbol{q}_e; I_x; I_y; I_z]$, and the output layers $\tilde{\boldsymbol{C}}_1$ and $\tilde{\boldsymbol{C}}_2$ are the estimated values of the actuator deviation faults $\boldsymbol{C}_1$ and actuator gain faults coefficient $\boldsymbol{C}_2$ respectively. The initial parameters setting of the RBF neural network is a problem that needs attention. The initial values of the center vector $\boldsymbol{G}_i$ and the base width vector $\boldsymbol{B}$ are generally set within the range of the input vector. The weight $\boldsymbol{W}$ can randomly select a group of initial values, which is not easy to be too large. In addition, during the use of the RBF neural network, the above parameters need to undergo a supervised learning process. In order to further improve the approximation ability of RBF, the particle swarm optimization (PSO) algorithm is used to optimize its parameters in this paper, and the specific steps are as follows:

First, as shown in Figure 3, the performance index function is selected as follows:

$$E(k) = \frac{1}{2}[y(k) - y_m(k)]^2 \tag{17}$$

where, $y(k)$ is the expected value, $y_m(k)$ is the estimated value.

Second, the PSO algorithm is used to optimize RBF neural network parameters. Due to space limitation, the detailed

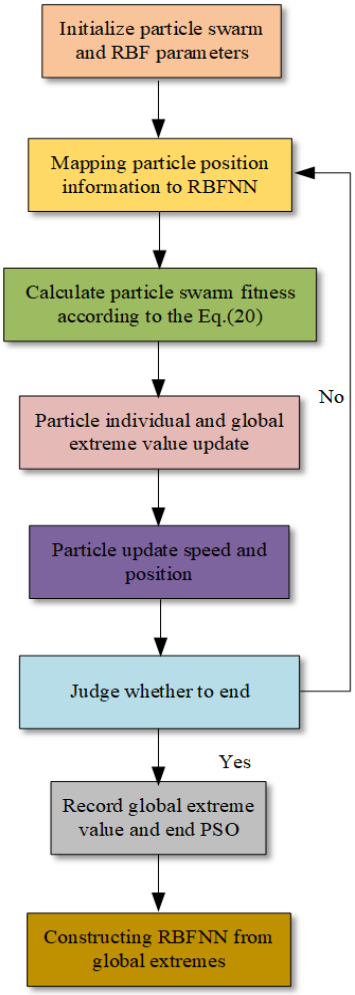


**FIGURE 4.** PSO-RBF neural network.

algorithm of the PSO can refer to relevant literature [44]. Parameters $\boldsymbol{G}_i$, $\boldsymbol{B}$, and $\boldsymbol{W}$ are taken as free-moving particles, and the position of particles is expressed in vector form as

$$\boldsymbol{X} = \left[\mathrm{w}_{11}, w_{12}, \ldots, w_{np}, b_1, b_2, \ldots, b_m, g_{11}, g_{12}, \ldots, g_{mn}\right]^{\mathrm{T}} \tag{18}$$

The particle space dimension is set to

$$D = (2 + m)\, n \tag{19}$$

In order to further reduce the estimation error of RBF neural network, the mean root square error of the RBF neural network performance index is taken as the fitness function of PSO:

$$f = \sqrt{\frac{1}{p}\sum_{k=1}^{p} E(k)} \tag{20}$$

The process of PSO algorithm optimizing RBF neural network model is shown in Figure 4.

### B. EXTENDED STATE OBSERVER (ESO)

ESO [45], [46] is the key link in ADRC technology. Traditional ESO usually attributes the uncertainty problems such as system identification and external disturbance to interference suppression, but this type of full compensation behavior may lead to overexcitation when the system has faults [47]. Therefore, based on the traditional ESO, this study fully considers the rationality of disturbance compensation and adopts the method of combining ESO and RBF neural networks to estimate the uncertainty of the system. The specific design ideas of the ESO are as follows:

First, the uncertainty of ESO estimation is expanded to a new variable $\boldsymbol{x}$.

$$\begin{aligned}\boldsymbol{x} = \frac{1}{2}\begin{bmatrix} 0 & -\Delta \boldsymbol{h}_e^{\mathrm{T}} \\ -\Delta \boldsymbol{h}_e & -\Delta \tilde{\boldsymbol{h}}_e \end{bmatrix} \boldsymbol{q}_e \\ + \frac{1}{2}\begin{bmatrix} -\boldsymbol{q}_e^T \\ q_{e0}\boldsymbol{I}_{3\times 3} + \tilde{\tilde{\boldsymbol{q}}}_e \end{bmatrix} (\boldsymbol{J} + \Delta \boldsymbol{J})^{-1} \boldsymbol{w}\end{aligned} \tag{21}$$

Secondly, the third-order ESO is designed as follows:

$$\begin{cases} \boldsymbol{e}_1 = z_1 - \boldsymbol{q}_e \\ \dot{z}_1 = z_2 - \beta_{01}\boldsymbol{e}_1 \\ \dot{z}_2 = \boldsymbol{f}_0 + z_3 - \beta_{02}\ \mathrm{fal}\ (\boldsymbol{e}_1, \alpha_1, \delta) + C_0 \boldsymbol{\tau}_c + \zeta \\ \dot{z}_3 = -\beta_{03}\ \mathrm{fal}\ (\boldsymbol{e}_1, \alpha_2, \delta) \end{cases} \tag{22}$$

where, $z_1$, $z_2$, and $z_3$ are the estimated values of $\boldsymbol{q}_e$, $\dot{\boldsymbol{q}}_e$, and $\boldsymbol{x}$ respectively; $\beta_{01}$, $\beta_{02}$, and $\beta_{03}$ are the parameter of ESO; $\zeta$ is the sum of the actuator deviation faults $\boldsymbol{C}_1$ and actuator gain faults $\boldsymbol{C}_2$ estimated by RBF neural network; the specific expression of the fal(·) function is as follows:

$$\mathrm{fal}\,(\boldsymbol{e}_1, \alpha_i, \delta) = \begin{cases} |\boldsymbol{e}_1|^{\alpha_i}\, \mathrm{sign}\,(\boldsymbol{e}_1), & |\boldsymbol{e}_1| > \delta \\ \boldsymbol{e}_1 / \delta^{1-\alpha_i}, & |\boldsymbol{e}_1| \le \delta \end{cases} \tag{23}$$

where, the nonlinear function fal(·) has characteristics of "small error, large gain; large error, small gain" when the degree of nonlinearity of the function $0 < \alpha_i < 1$. When $\alpha_i = 1$, the nonlinear function fal(·) turns into a linear one, Eq. (23) is called LESO [48], [49]. The parameter $\delta > 0$ represents the interval length of the linear segment.

For the parameter selection of the ESO, this paper refers to the determination method in [45]. When the step size is $h$, the function parameters selection are $\alpha_i = 1/2^{i-1}$ and $\delta = h$ generally, and the parameter $\beta_{0i}$ is related to the step size, the approximate formula is as follows:

$$\begin{aligned} \beta_{01} &\approx \frac{1}{h} \\ \beta_{02} &\approx \frac{1}{1.6h^{1.5}} \\ \beta_{03} &\approx \frac{1}{8.6h^{2.2}} \end{aligned} \tag{24}$$

### C. IMPROVED NONLINEAR STATE ERROR FEEDBACK (NLSEF)

The error equation is established as follows:

$$\begin{cases} \boldsymbol{e} = \boldsymbol{q}_{ed} - \boldsymbol{q}_e \\ \dot{e} = \dot{q}_{ed} - \dot{\boldsymbol{q}}_e \end{cases} \tag{25}$$

where, $\boldsymbol{q}_{ed}$ is the expected value of the error quaternion $\boldsymbol{q}_e$. When the attitude quaternion of the tracking spacecraft coincides with the expected attitude quaternion, the expected error quaternion and its derivative are expressed as $\boldsymbol{q}_{ed} = \begin{bmatrix} 1 & 0 & 0 & 0 \end{bmatrix}$ and $\dot{\boldsymbol{q}}_{ed} = \begin{bmatrix} 0 & 0 & 0 & 0 \end{bmatrix}$.

In the design of NLSEF, this study adopts a FNTSMS to replace the traditional ADRC design form. The sliding mode hyperplane is designed as follows:

$$s = \dot{e} + k_1 e + k_2 S_{\text{au}} \tag{26}$$

where, $k_1 > 0$, $k_2 > 0$, $S_{\text{au}} = \begin{bmatrix} S_{\text{au1}} & S_{\text{au2}} & S_{\text{au3}} & S_{\text{au4}} \end{bmatrix}^{\text{T}}$. The expression of $S_{\text{aui}}$ is:

$$S_{\text{aui}} = \begin{cases} e_i^r, \bar{S}_i = 0 \\ e_i^r, \bar{S}_i \neq 0 \text{ and } |e_i| \geq \gamma \\ t_1 e_i + t_2 \text{ sgn}(e_i) e_i^2, \ \bar{S}_i \neq 0 \text{ and } |e_i| < \gamma \end{cases} \quad (i = 1, \ldots 4) \tag{27}$$

where, $\bar{S}_i = \dot{e}_i + k_1 e_i + k_2 e_i^r$, $0 < r = \frac{r_1}{r_2} < 1$, $r_1$ and $r_2$ denote positive odd numbers; $\gamma > 0$ is a small constant; $t_1 = (2 - \frac{r_1}{r_2}) \gamma^{\frac{r_1}{r_2} - 1}$; $t_2 = (\frac{r_1}{r_2} - 1) \gamma^{\frac{r_1}{r_2} - 2}$; and sgn$(\cdot)$ is a symbolic function.

The expression of $\dot{S}_{\text{au}} = \begin{bmatrix} \dot{S}_{\text{au1}} & \dot{S}_{\text{au2}} & \dot{S}_{\text{au3}} & \dot{S}_{\text{au4}} \end{bmatrix}^{\text{T}}$ is:

$$\dot{S}_{\text{aui}} = \begin{cases} r e_i^{r-1} \dot{e}_i, \bar{S}_i = 0 \\ r e_i^{r-1} \dot{e}_i, \bar{S}_i \neq 0 \text{ and } |e_i| \geq \gamma \\ t_1 \dot{e}_i + 2 t_2 \text{ sgn}(e_i) e_i \dot{e}_i, \ \bar{S}_i \neq 0 \text{ and } |e_i| < \gamma \end{cases} \quad (i = 1, \ldots 4) \tag{28}$$

The derivative of Eq. (26) is:

$$\dot{s} = \ddot{e} + k_1 \dot{e} + k_2 \dot{S}_{au} \tag{29}$$

The exponential control law is:

$$\dot{s} = -\rho_1 s - \rho_2 |s|^k \text{ sgn}(s) \tag{30}$$

where, $k \in \mathbb{R}^+$, and meets $0 < k < 1$; $\rho_1$ and $\rho_2 \in \mathbb{R}^+$.

The control law obtained from simultaneous Eq. (29) and Eq. (30) is as follows:

$$\tau_0 = -\text{inv}(C_0) \Big[ F + f_0 + C_1 + C_2 + k_1 \dot{e} + k_2 \dot{S}_{au} + \rho_1 s + \rho_2 |s|^k \text{ sgn}(s) \Big] \tag{31}$$

The control law after ESO and RBF neural network estimation and compensation is:

$$\tau_c = -\text{inv}(C_0) \Big[ z_3 + f_0 + \zeta + k_1 \hat{\dot{e}} + k_2 \hat{\dot{S}}_{\text{au}} + \rho_1 \hat{s} + \rho_2 \left| \hat{s} \right|^k \text{sgn}(\hat{s}) \Big] \tag{32}$$

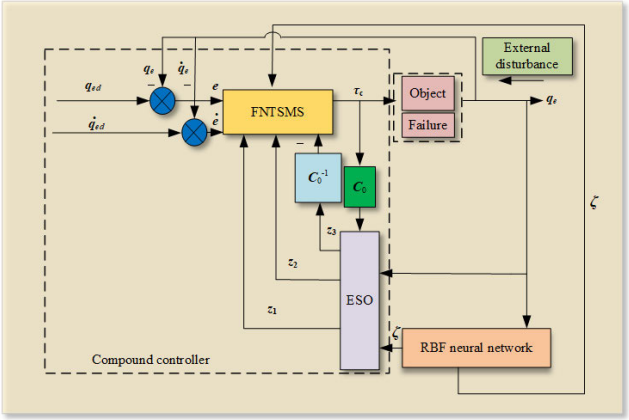


**FIGURE 5.** Control scheme diagram.

where, $\hat{e} = \boldsymbol{q}_{ed} - \boldsymbol{z}_1$, $\hat{\dot{e}} = \dot{\boldsymbol{q}}_{ed} - \boldsymbol{z}_2$, $\hat{s} = \hat{\dot{e}} + k_1 \hat{e} + k_2 \hat{S}_{\text{au}}$, $\hat{S}_{au}$ and $\hat{\dot{S}}_{au}$ are the results of substituting $\hat{e}$ and $\hat{\dot{e}}$ into Eq. (27) and Eq. (28) respectively.

The overall framework of the controller designed in this study is shown in Figure 5.

*Remark 2:* The controller designed in this paper is different from [29] and [50] in that the sliding mode surface in this chapter is a FNTSMS, which not only avoids singular problems, but also includes the advantages of common sliding mode surface and nonsingular sliding mode surface. The difference between uncertainty compensation and [17] is that the nonlinear uncertainty caused by external interference is estimated by ESO, and the uncertainty caused by multiplicative fault and additive fault is estimated by RBF neural network, so that each uncertainty becomes clearer.

### D. STABILITY ANALYSIS OF CLOSED-LOOP SYSTEM

Firstly, the stability analysis of ESO refers to the convergence and stability analysis method of linear/nonlinear switching extended state observer in [46]. The nonlinear function can be regarded as a linear function with variable gain. According to the root locus method, combined with specific parameter settings and physical processes, judge whether the root of the characteristic equation is located on the left side of the [S] plane. If so, the system is stable. The stability of ESO will be further verified in simulation.

Secondly, the stability of the closed-loop system is proved as follows:

*Lemma 1 [51]:* Consider the system $\dot{\boldsymbol{x}} = f(\boldsymbol{x})$, $\boldsymbol{x} \in \mathbb{R}^n$, $\forall \boldsymbol{x}(0)$, if there exists a continuous Lyapunov function $V(\boldsymbol{x}) \geq 0$ in $\mathbb{R}^n$, and scalars $c_1 > 0$, $\chi > 0$, $0 < p < 1$, such that

$$\dot{\boldsymbol{V}}(\boldsymbol{x}) \leq -c_1 \boldsymbol{V}^p(\boldsymbol{x}) + \chi \tag{33}$$

Then, the system $\dot{\boldsymbol{x}} = f(\boldsymbol{x})$ is the global practical finite-time bounded (GPFB), and the trajectory of the closed-loop system converges to a compact set containing the origin $\lim_{t \to T} \boldsymbol{x} \in \left\{ \boldsymbol{x} : V^p(\boldsymbol{x}) \leq \frac{\chi}{(1-q)c_1} \right\}$ in a finite time $\boldsymbol{T}_{\text{s}}$. The settling time $\boldsymbol{T}_{\text{s}}$ is given by Eq. (34), $0 < q < 1$ is scalar, and $\boldsymbol{V}(\boldsymbol{x}(0))$ is

the initial value of $\boldsymbol{V}(\boldsymbol{x})$.

$$T_s = \frac{1}{(1-p)qc_1}\left[V^{1-p}(x(0)) - \left(\frac{\chi}{(1-q)c_1}\right)^{(1-p)/p}\right] \tag{34}$$

*Lemma 2 [52]:* For variables $x, y \in \mathbb{R}$, there exists $\alpha > 0$, and scalars $p > 1, q > 1, (q-1)(p-1) = 1$, there is inequality

$$xy \le \frac{\alpha^p}{p}|x|^p + \frac{1}{q\alpha^q}|y|^q \tag{35}$$

*Theorem 1:* For the space tumbling target synchronous flying around system, the relative attitude kinematics and dynamics equation is Eq. (14), considering the simultaneous multiplicative and additive faults of the actuator, ESO and RBF neural network are used to estimate and compensate the system faults, uncertainty, external disturbance, and saturated nonlinear terms online, and the nonlinear state feedback law is designed in combination with the FNTSMS Eq. (32). The sliding mode surface converges to region in finite time, so the system state variables tend to a small region containing the origin in a limited time.

*Proof:* The positive-definite candidate of the Lyapunov function is selected as follows:

$$\boldsymbol{V} = {}^1\!/_2 \boldsymbol{s}^T \boldsymbol{s} \tag{36}$$

We take the derivative of Eq. (36), and substitute the estimation error $\psi$ of the ESO and RBF neural network for the state variables and unknown parts, Eq. (14) and Eq. (32) into it.

$$\begin{aligned}
\dot{V} &= s^T(\ddot{e} + k_1\dot{e} + k_2\dot{S}_{au}) \\
&= s^T(F + f_0 + C_1 + C_2 + C_0\tau_c + k_1\dot{e} + k_2\dot{S}_{\mathrm{au}}) \\
&= s^T(\psi - \rho_1 s - \rho_2 \|s\|^k \operatorname{sgn}(s)) \\
&= s^T\psi - \rho_1\|s\|^2 - \rho_2\|s\|^{k+1} \\
&\le \|s\|\,\|\psi\| - \rho_1\|s\|^2 - \rho_2\|s\|^{k+1} \\
&\le \|s\|\,\|\psi\| - \rho_2\|s\|^{k+1}
\end{aligned} \tag{37}$$

According to lemma 2, there is the following inequality.

$$\|s\|\,\|\psi\| \le \frac{\varepsilon^{k+1}}{k+1}\|s\|^{k+1} + \frac{k}{(k+1)\varepsilon^{\frac{k+1}{k}}}\|\psi\|^{\frac{k+1}{k}} \tag{38}$$

where, $\varepsilon > 0$.

Substitute Eq. (38) into Eq. (37).

$$\begin{aligned}
\dot{V} &\le \frac{\varepsilon^{k+1}}{k+1}\|s\|^{k+1} + \frac{k}{(k+1)\varepsilon^{\frac{k+1}{k}}}\|\psi\|^{\frac{k+1}{k}} - \rho_2\left\|s^2\right\|^{\frac{k+1}{2}} \\
&= -(\rho_2 - \frac{\varepsilon^{k+1}}{k+1})\left\|s^2\right\|^{\frac{k+1}{2}} + \frac{k}{(k+1)\varepsilon^{\frac{k+1}{k}}}\|\psi\|^{\frac{k+1}{k}} \\
&= -2^{\frac{k+1}{2}}(\rho_2 - \frac{\varepsilon^{k+1}}{k+1})V^{\frac{k+1}{2}} + \frac{k}{(k+1)\varepsilon^{\frac{k+1}{k}}}\|\psi\|^{\frac{k+1}{k}}
\end{aligned} \tag{39}$$

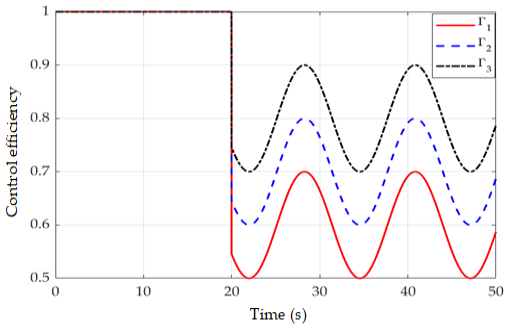


**FIGURE 6.** Control efficiency.

Taking $k$ and $\rho_2$ as satisfying $2^{\frac{k+1}{2}}(\rho_2 - \frac{\varepsilon^{k+1}}{k+1}) \ge \sigma$, where, $\sigma$ is a positive constant, Eq. (39) can be rewritten as follows:

$$\dot{V} \le -\sigma V^{\frac{k+1}{2}} + \frac{k}{(k+1)\varepsilon^{\frac{k+1}{k}}}\|\psi\|^{\frac{k+1}{k}} \tag{40}$$

According to Lemma 1, the trajectory of the FNTSMS converges to a small region containing $\boldsymbol{A} = \left\{\boldsymbol{s} : \|\boldsymbol{s}\|^{k+1} \le 2^{\frac{k+1}{2}}\boldsymbol{B}_0\right\}$ in a finite time $T_{\mathrm{s}}$.

$$T_{\mathrm{s}} = \frac{2}{(1-k)q\sigma}\left[V^{\frac{1-k}{2}}(s(0)) - B_0^{\frac{1-k}{1+k}}\right] \tag{41}$$

where, $0 < q < 1$, $\boldsymbol{B}_0$ is a normal number, the expression is $\boldsymbol{B}_0 = \frac{k}{(1-q)\sigma(k+1)\varepsilon^{\frac{k+1}{k}}}\|\psi\|^{\frac{k+1}{k}}$, and $\boldsymbol{B}_0$ can be sufficiently small by properly adjusting the parameters.

## IV. SIMULATION VERIFICATION

In this study, the nonlinear feedback form of FNTSMS is used to improve the traditional ADRC, and the ESO and RBF neural network are combined to estimate the system uncertainty respectively, so that the attitude FTC of the space tumbling target is achieved, and the robustness and effectiveness of the above method are verified by simulation analysis.

The main parameters of the tracking spacecraft are as follows:

The nominal value of the inertia tensor is $J_0 = \operatorname{diag}\{58\ 55\ 49\}$ kg.m$^2$.

The uncertainty of the inertia tensor is $\Delta J = \operatorname{diag}\{\sin(0.1t)\ 2\sin(0.2t)\ 3\sin(0.3t)\}$ kg.m$^2$.

The initial attitude quaternion is $q = \begin{bmatrix}1\ 0\ 0\ 0\end{bmatrix}^{\mathrm{T}}$. The attitude angular velocity at the initial time is $\omega = \begin{bmatrix}0\ 0\ 0\end{bmatrix}^{\mathrm{T}}$ rad/s.

The maximum control torque is set as 30 N.m.

The external disturbance is $w = [2 + 3\cos(3t)\ 2\sin(1.5t) + 3\cos(1.5t)\ 1 + 4\sin(2t)]^T$ N.m.

When the time is less than 20 s, the additive failure error is $\bar{\tau}_c = [0\ 0\ 0]^T$; When the time exceeds 20 s, the additive failure error is $\bar{\tau}_c = [-3(1-e^{-2t})\ -3.2(1-e^{-2t})\ -3.4(1-e^{-2t})]^T$.

The control efficiency is $\Gamma = \operatorname{diag}\{\rho_1, \ldots, \rho_n\}$, as shown in Figure 6. When the time is less than 20 s, $\rho_1 = \rho_2 = \rho_3 = 1$ occurs. When the time exceeds 20 s,

**TABLE 1. Parameter value.**

| Parameter | Value | Parameter | Value |
|---|---|---|---|
| $\beta_{01}$ | 100 | $k_1$ | 1.2 |
| $\beta_{02}$ | 600 | $k_2$ | 0.1 |
| $\beta_{03}$ | 3000 | $r_1$ | 3 |
| $\alpha_1$ | 0.5 | $r_2$ | 5 |
| $\alpha_2$ | 0.25 | $k$ | 0.5 |
| $\delta$ | 0.01 | $\rho_1$ | 0.4 |
| $\gamma$ | 0.001 | $\rho_2$ | 0.001 |

the actuator starts to fail, and the specific expression of $\Gamma$ is as follows:

$$\begin{cases} \rho_1 = 0.6 + 0.1\sin(0.5t) \\ \rho_2 = 0.7 + 0.1\sin(0.5t) \\ \rho_3 = 0.8 + 0.1\sin(0.5t) \end{cases} \quad (t >= 20s) \qquad (42)$$

The ESO parameter selection criteria refer to [40], and other controller parameters are set according to their value ranges to keep the controller stable by cut-and-trial method. The parameter values of the designed composite controller and ESO are listed in Table 1.

In this study, the simulated space tumbling target is in the case of regular precession, and the simulated flying around scene follows the rotating axis to fly around synchronously. The parameters involved are the same as those in the literature [29], therefore, the expected attitude quaternion and expected angular velocity always change with time, as shown in Figure 7.

### A. ESO CONVERGENCE AND RBF ESTIMATION ABILI-TY

Combining the parameter values in Table 1 and the specific control process of the controlled object under the FTNSMS control scheme, the root locus method is used to draw the moving locus of the closed-loop characteristic root of the system with the error on the [s] plane. As shown in Figure 8, due to space limitation, one root locus graph is displayed. When $\boldsymbol{e}_1$ changes, the closed-loop pole is always located on the left half plane of [S], that is, for any $\boldsymbol{e}_1$ value, the system will gradually tend to balance, which proves that the ESO designed in this paper has good convergence.

The approximation ability of RBF neural network and the estimation ability of ESO are shown in Figure 9. It can be seen from (a), RBF neural network can approach the nonlinear uncertainty part $\boldsymbol{C}_1$ caused by the actuator drift fault, the change of inertia moment, and the physical property limitation with high accuracy. It can be seen from (b), RBF neural network can approach the nonlinear part $\boldsymbol{C}_2$ caused by the uncertainty of actuator efficiency, inertia, and torque with high accuracy. It can be seen from (c), ESO has a strong estimation energy for the unknown nonlinear part $\boldsymbol{F}$ of the system caused by the external disturbance and the uncertainty of the inertia moment.

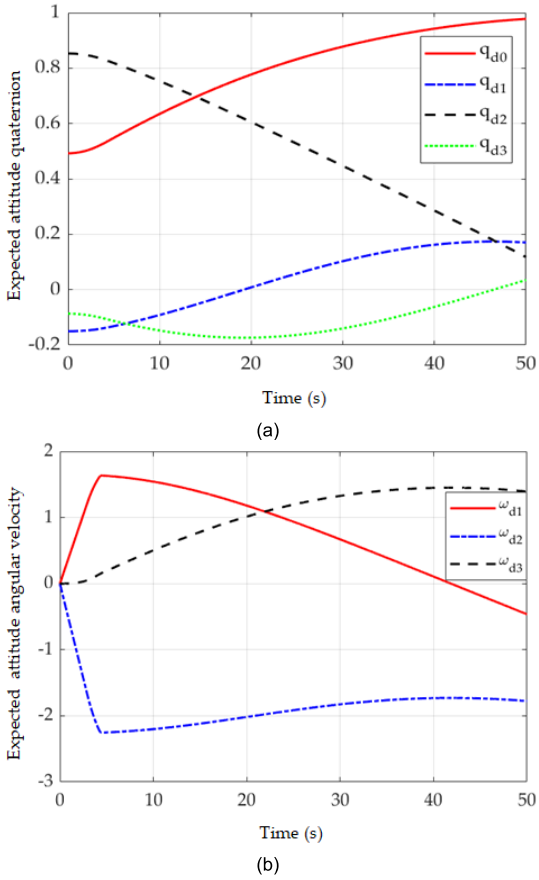


**FIGURE 7. Expected attitude curves with time. (a) Expected attitude quaternion curve. (b) Expected attitude angular velocity curve.**

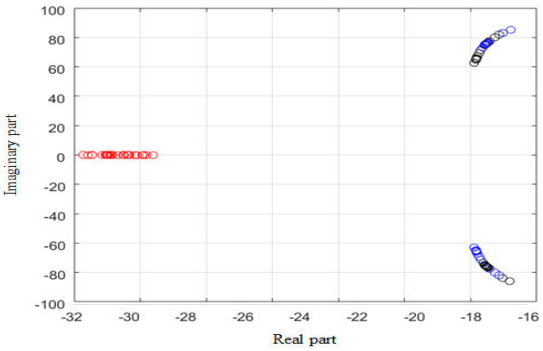


**FIGURE 8. Root locus of error.**

### B. COMPARISON BETWEEN FNTSMS AND LSMS CON-TROL SCHEMES

To further verify the superiority of the ADRC based FNTSMS attitude FTC scheme designed in this study, consider the same constraints as this study (system inertia uncertainty, external disturbance, actuator saturation, and actuator fault), and compare it with the linear sliding mode surface (LSMS) scheme designed in [31].

The error attitude quaternion changes with time under the two schemes as shown in Figure 10. It can be seen from

**TABLE 2.** Values of MAE.

| Name | MAE$q_{e0}$ | MAE$q_{e1}$ | MAE$q_{e2}$ | MAE$q_{e3}$ | MAE$\omega_{e1}$ | MAE$\omega_{e2}$ | MAE$\omega_{e3}$ |
|---|---|---|---|---|---|---|---|
| LSMS | 0.067772 | 0.017418 | 0.189858 | 0.009542 | 0.408142 | 2.388248 | 0.085882 |
| FNTSMS | 0.020578 | 0.010502 | 0.057488 | 0.005854 | 0.408098 | 2.387004 | 0.156452 |

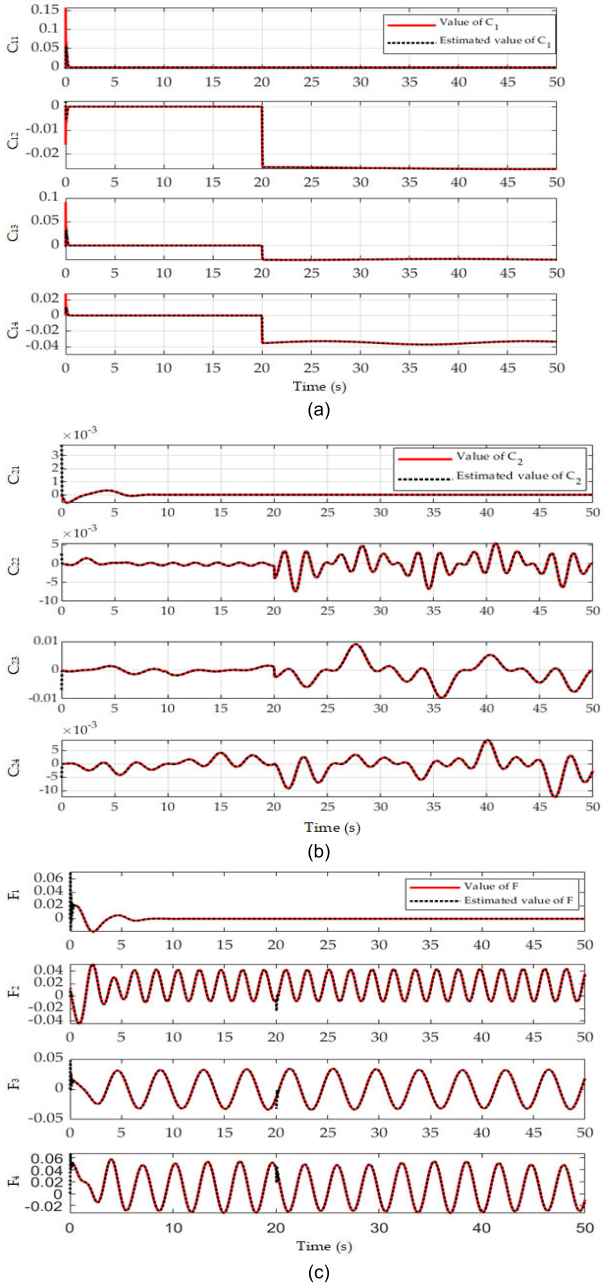


**FIGURE 9.** Estimation curves by RBF neural network and ESO. (a) Estimation curves of $C_1$ using RBF neural network. (b) Estimation curves of $C_2$ using RBF neural network. (c) Estimation curves of F using ESO.

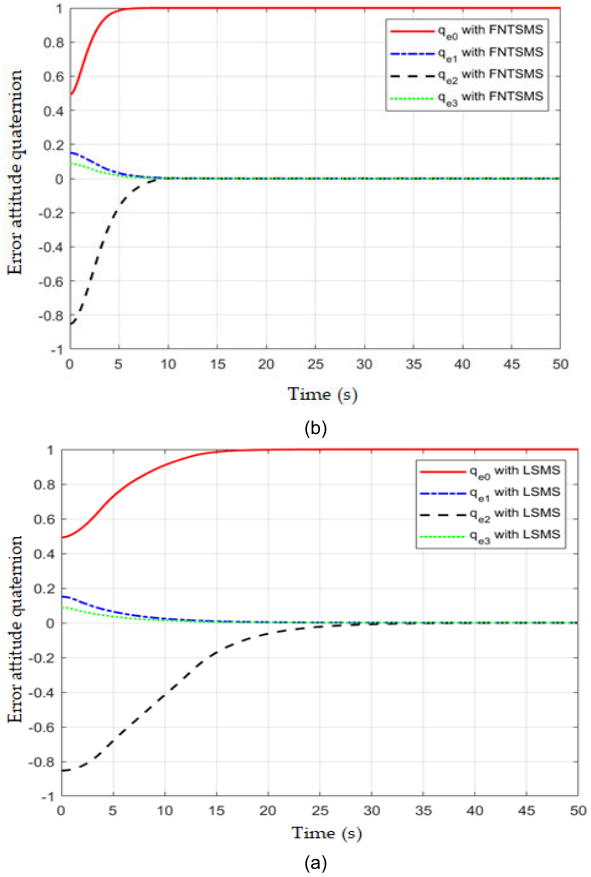


**FIGURE 10.** Curves of error attitude quaternion with time. (a) The FNTSMS control scheme. (b) The LSMS control scheme.

(a) that the error attitude quaternion based on the FNTSMS control scheme converges to the expected value in 10 seconds and can efficiently track the attitude of the space tumbling target with high accuracy. It can be seen from (b) that the error attitude quaternion based on LSMS control scheme converges to the expected value in 40 seconds, with a longer convergence speed and lower convergence accuracy.

The error angular velocity changes with time under the two schemes is shown in Figure 11. It can be seen from (a) that the error angular velocity based on the FNTSMS control scheme converges to the expected value in 10 seconds. It can be seen from (b) that the error angular velocity based on the LSMS control scheme converges to the expected value in 40 seconds and has a longer convergence time. Although the convergence precision of the two schemes is similar, the curve based on the FNTSMS control scheme is smoother.

The control torque changes with time under the two schemes is shown in Figure 12. It can be seen from (a) that the control torque based on FNTSMS control scheme shows a smooth control curve after reaching saturation in a short

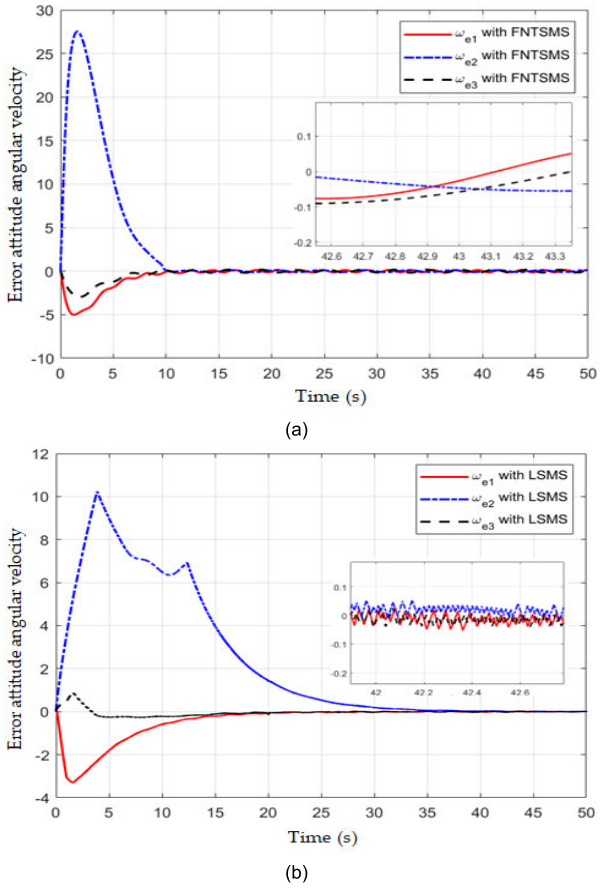


**FIGURE 11.** Curves of error angular velocity with time. (a) The FNTSMS control scheme. (b) The LSMS control scheme.

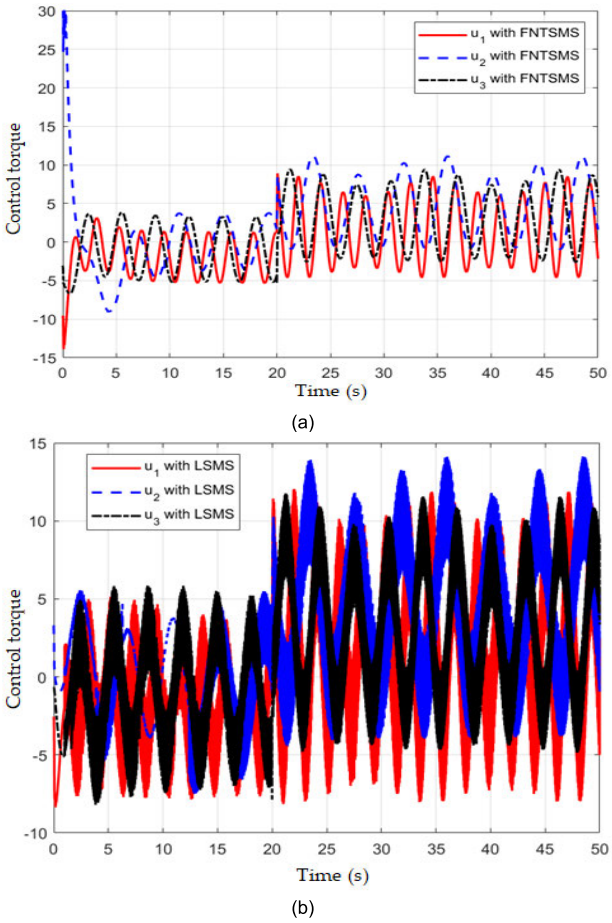


**FIGURE 12.** Curves of control torque with time. (a) The FNTSMS control scheme. (b) The LSMS control scheme.

time at the initial time. When the actuator fails at 20 seconds, the control torque suddenly increases to a certain extent and remains stable. It can be seen from (b) that the control torque based on LSMS control scheme has no saturation at the initial time, but chattering is obvious.

To measure the control effect further, we introduce the mean absolute error (MAE) [53] as a control index. The expression of MAE is as follows:

$$\mathrm{MAE} = \frac{1}{t_\infty - t_0} \int_{t_0}^{t_\infty} |e(t)| dt \tag{43}$$

The MEA values of the error attitude quaternion and error angular velocity of the control law designed based on the FNTSMS and LSMS are listed in Table 2. It is noted that, compared with LSMS, the FNTSMS based control scheme is larger in the third component of error angular velocity (scribed line in Table 2). Even so, the FNTSMS based control scheme is more reasonable when evaluating performance indicators from the overall perspective. Considering the convergence speed, control effect and control curve smoothness, the system response based on FNTSMS control is preferred in practice.

## V. CONCLUSION

In this study, for the space tumbling target whose attitude and angular velocity are always changing, when the relative error attitude dynamics equation is established, a new RLOS coordinate system that is more practical is selected. Aiming at the uncertainty and fault problems that may occur in engineering practice, the additive and multiplicative faults of the system are estimated online by using the nonlinear function approximation ability of RBF neural network, and the total disturbance and uncertainty of the system are estimated by using ESO, both of which complete the active fault tolerance and interference suppression control of the system. The strict finite time stability proof process is provided for the designed controller under the Lyapunov framework to obtain the expressions of the convergence time and the convergence region of the sliding mode surface, and then the finite time convergence conclusion of the system state is obtained. Finally, comparative simulation experiments and data comparison are set up to prove the effectiveness and superiority of the controller designed in this study. In addition, referring to the current mature physical experiment platform simulation method [54], establishing a ground suspension experiment

platform for the motion control of spacecraft tumbling target is also one of our research goals, which further demonstrates and expands the research results in this study.

## REFERENCES

[1] R. Miller, *Orbital Debris Quarterly News*, NASA, Washington, DC, USA, 2021. [Online]. Available: http://ufdc.ufl.edu/AA00058853/00095

[2] S. Bandyopadhyay, S.-J. Chung, and F. Y. Hadaegh, "Nonlinear attitude control of spacecraft with a large captured object," *J. Guid., Control, Dyn.*, vol. 39, no. 4, pp. 754–769, Apr. 2016, doi: 10.2514/1.G001341.

[3] L. Zhang, S. Qian, S. Zhang, and H. Cai, "Research on angles-only/SINS/CNS relative position and attitude determination algorithm for a tumbling spacecraft," *Proc. Inst. Mech. Eng., G, J. Aerosp. Eng.*, vol. 231, no. 2, pp. 218–228, 2017, doi: 10.1177/0954410016636153.

[4] Y. She, J. Sun, S. Li, W. D. Li, and T. Song, "Quasi-model free control for the post-capture operation of a non-cooperative target," *Acta Astronautica*, vol. 147, pp. 59–70, Jun. 2018, doi: 10.1016/j.actaastro.2018.03.041.

[5] M. Wang, J. Luo, J. Yuan, and U. Walter, "Detumbling strategy and coordination control of kinematically redundant space robot after capturing a tumbling target," *Nonlinear Dyn.*, vol. 92, no. 3, pp. 1023–1043, May 2018, doi: 10.1007/s11071-018-4106-4.

[6] B. L. Keith, R. D. Leach, and M. B. Alexander, "Spacecraft system failures and anomalies attributed to the natural space environment," presented at the Space Programs Technol. Conf., Huntsville, AL, USA, 1996.

[7] K. D. Gunter. (2021). *Spaceflight Accidents*. [Online]. Available: https://space.skyrocket.de/doc_sat/accidents_crewed.htm

[8] P. Huang, Y. Lu, M. Wang, Z. Meng, Y. Zhang, and F. Zhang, "Postcapture attitude takeover control of a partially failed spacecraft with parametric uncertainties," *IEEE Trans. Autom. Sci. Eng.*, vol. 16, no. 2, pp. 919–930, Apr. 2019, doi: 10.1109/TASE.2018.2875139.

[9] J. Kurien and M. D. R. Moreno, "Intrinsic hurdles in applying automated diagnosis and recovery to spacecraft," *IEEE Trans. Syst., Man, Cybern., A, Syst. Humans*, vol. 40, no. 5, pp. 945–958, Sep. 2010, doi: 10.1109/TSMCA.2010.2052035.

[10] C. Stephen. (2021). *Attitude Control Failures Led to Break-up of Japanese Astronomy Satellite*. [Online]. Available: https://spaceflightnow.com/2016/04/18/spinning-japanese-astronomy-satellite-may-be-beyond-saving

[11] C. P. Bechlioulis and G. A. Rovithakis, "Robust adaptive control of feedback linearizable MIMO nonlinear systems with prescribed performance," *IEEE Trans. Autom. Control*, vol. 53, no. 9, pp. 2090–2099, Oct. 2008, doi: 10.1109/TAC.2008.929402.

[12] K. D. Kumar, "Robust attitude stabilization of spacecraft subject to actuator failures," *Acta Astronautica*, vol. 68, nos. 7–8, pp. 1242–1259, Apr. 2011, doi: 10.1016/j.actaastro.2010.10.017.

[13] D. Ran, X. Chen, A. de Ruiter, and B. Xiao, "Adaptive extended-state observer-based fault tolerant attitude control for spacecraft with reaction wheels," *Acta Astronautica*, vol. 145, pp. 501–514, Apr. 2018, doi: 10.1016/j.actaastro.2018.01.021.

[14] X. H. Liang, Q. Wang, C. H. Hu, and C. Y. Dong, "Observer-based $H_\infty$ fault-tolerant attitude control for satellite with actuator and sensor faults," *Aerosp. Sci. Technol.*, vol. 95, Dec. 2019, Art. no. 105424, doi: 10.1016/j.ast.2019.105424.

[15] H. Gui and G. Vukovich, "Adaptive integral sliding mode control for spacecraft attitude tracking with actuator uncertainty," *J. Franklin Inst.*, vol. 352, no. 12, pp. 5832–5852, Dec. 2015, doi: 10.1016/j.jfranklin.2015.10.001.

[16] A. H. Zhang, Y. C. Wang, Z. Q. Zhang, and H. R. Karimi, "Robust control allocation for spacecraft attitude stabilization under actuator faults and uncertainty," *Math. Problems Eng.*, vol. 2014, p. 12, 2014, doi: 10.1155/2014/789327.

[17] B. Y. Huo, "Research on fault-tolerant attitude control methods for spacecraft," Ph.D. dissertation, Beijing Inst. Technol., Beijing, China, 2017.

[18] Q. Liu, M. Liu, and J. Yu, "Adaptive fault-tolerant control for attitude tracking of flexible spacecraft with limited data transmission," *IEEE Trans. Syst., Man, Cybern., Syst.*, vol. 51, no. 7, pp. 4400–4408, Jul. 2021, doi: 10.1109/TSMC.2019.2932225.

[19] Q. Hu, L. Xiao, and C. Wang, "Adaptive fault-tolerant attitude tracking control for spacecraft with time-varying inertia uncertainties," *Chin. J. Aeronaut.*, vol. 32, no. 3, pp. 674–687, Mar. 2019, doi: 10.1016/j.cja.2018.12.015.

[20] J. Liu, H. Li, Y. Luo, and J. Zhang, "Robust adaptive relative position and attitude integrated control for approaching uncontrolled tumbling spacecraft," *Proc. Inst. Mech. Eng., G, J. Aerosp. Eng.*, vol. 234, no. 2, pp. 361–374, Feb. 2020, doi: 10.1177/0954410019866282.

[21] B. Y. Jiang, Q. L. Hu, Z. B. Shi, and G. F. Ma, "Relative position and attitude coupled controller design for approaching and docking with a freely tumbling target," *J. Astronaut.*, vol. 35, no. 1, pp. 54–60, 2014, doi: 10.3873/j.issn.1000-1328.2014.01.007.

[22] Y. Liu, Y. Liang, K. Li, J.-Y. Zhou, and J.-T. Li, "Control strategy design for forced fly-around against the tumbling target based on differential geometric principle," *Aerosp. Syst.*, vol. 3, no. 1, pp. 9–19, Mar. 2020, doi: 10.1007/s42401-020-00043-0.

[23] Z. J. Chen, Y. Zhao, Y. Z. Bai, D. C. Ran, and L. He, "Extended-state-observer-based terminal sliding mode tracking control for synchronous fly-around with space tumbling target," *Math. Problems Eng.*, vol. 2019, Nov. 2019, Art. no. 5791579, doi: 10.1155/2019/5791579.

[24] Y. S. Huang, D. Tian, H. Y. Li, R. H. Jiao, and F. Li, "A trajectory planning and tracking algorithm for the tumbling non-cooperative spacecraft approach, flying-around and obstacle avoidance," *Aerosp. Control Appl.*, vol. 47, pp. 1–8, Jan. 2021, doi: 10.3969/j.issn.1674-1579.2021.03.001.

[25] Q. Li, J. Yuan, and C. Sun, "Robust fault-tolerant saturated control for spacecraft proximity operations with actuator saturation and faults," *Adv. Space Res.*, vol. 63, no. 5, pp. 1541–1553, Mar. 2019, doi: 10.1016/j.asr.2018.11.004.

[26] Q. Hu, X. Shao, and W.-H. Chen, "Robust fault-tolerant tracking control for spacecraft proximity operations using time-varying sliding mode," *IEEE Trans. Aerosp. Electron. Syst.*, vol. 54, no. 1, pp. 2–17, Feb. 2018, doi: 10.1109/TAES.2017.2729978.

[27] B. Jiang, Q. Hu, and M. I. Friswell, "Fixed-time rendezvous control of spacecraft with a tumbling target under loss of actuator effectiveness," *IEEE Trans. Aerosp. Electron. Syst.*, vol. 52, no. 4, pp. 1576–1586, Aug. 2016, doi: 10.1109/TAES.2016.140406.

[28] W. L. Wang, L. Chen, Y. J. Lei, and Y. G. Liang, "Cooperative guidance and control for rendezvous with uncooperative target based on augment proportional navigation," presented at the 35th Chin. Control Conf., Chengdu, China, Jul. 2016.

[29] Y. H. Liu, "Research on guidance and control strategy of close-range relative motion against space tumbling target," M.S. thesis, Defense Technol. Univ, Changsha, China, 2018.

[30] J. H. Liu, H. Y. Li, L. Y. Yang, and L. Lu, "Control strategy of forced flying-around uncontrolled rotating targets," *Syst. Eng. Electron.*, vol. 40, pp. 2310–2319, Mar. 2019, doi: 10.3969/j.issn.1001-506X.2019.10.21.

[31] J. H. Liu and H. Y. Li, "Augmented proportional navigation control for approach to uncontrolled tumbling satellite," *Syst. Eng. Electron.*, vol. 40, pp. 2311–2316, Jun. 2018, doi: 10.3969/j.issn.1001-506X.2018.10.23.

[32] X. Lu, Y. Jia, Y. Fu, and F. Matsuno, "Constrained attitude control of uncertain spacecraft with appointed-time control performance," *IEEE Trans. Syst., Man, Cybern., Syst.*, vol. 53, no. 1, pp. 178–190, Jan. 2023, doi: 10.1109/TSMC.2022.3174845.

[33] B. J. Eddine, B. Elhassen, and K. Boulanouar, "Performance comparison of PD and Sliding adaptive controller method for rigid satellite attitude stabilization," presented at the 12nd ICAEE, Constantine, Algeria, Oct. 2022, doi: 10.1109/ICAEE53772.2022.9962094.

[34] J. F. He, Q. W. Li, and C. Liu, "Modified rodriguez parameters based event-triggered attitude control of flexible UCAV with uncertainties," presented at the 33th CCDC, Kunming, China, May 2021, doi: 10.1109/CCDC52312.2021.9602335.

[35] Y. Sun, Y. Gao, Y. Zhao, Z. Liu, J. Wang, J. Kuang, F. Yan, and J. Liu, "Neural network-based tracking control of uncertain robotic systems: Predefined-time nonsingular terminal sliding-mode approach," *IEEE Trans. Ind. Electron.*, vol. 69, no. 10, pp. 10510–10520, Oct. 2022, doi: 10.1109/TIE.2022.3161810.

[36] Z. Chu, F. Meng, D. Zhu, and C. Luo, "Fault reconstruction using a terminal sliding mode observer for a class of second-order MIMO uncertain nonlinear systems," *ISA Trans.*, vol. 97, pp. 67–75, Feb. 2020, doi: 10.1016/j.isatra.2019.07.024.

[37] B. Xiao, M. Huo, X. Yang, and Y. Zhang, "Fault-tolerant attitude stabilization for satellites without rate sensor," *IEEE Trans. Ind. Electron.*, vol. 62, no. 11, pp. 7191–7202, Nov. 2015, doi: 10.1109/TIE.2015.2432107.

[38] Y. Gao, J. Liu, G. Sun, M. Liu, and L. Wu, "Fault deviation estimation and integral sliding mode control design for Lipschitz nonlinear systems," *Syst. Control Lett.*, vol. 123, pp. 8–15, Jan. 2019, doi: 10.1016/j.sysconle.2018.08.006.

[39] W. Yu, X. Bu, and Z. Hou, "Security data-driven control for nonlinear systems subject to deception and false data injection attacks," *IEEE Trans. Netw. Sci. Eng.*, vol. 9, no. 4, pp. 2910–2921, Jul. 2022, doi: 10.1109/TNSE.2022.3173310.
[40] X. Wang, Y. Cao, B. Niu, and Y. Song, "A novel bipartite consensus tracking control for multiagent systems under sensor deception attacks," *IEEE Trans. Cybern.*, early access, Dec. 13, 2022, doi: 10.1109/TCYB.2022.3225361.
[41] B. Xiao, Q. Hu, and D. Wang, "Spacecraft attitude fault tolerant control with terminal sliding-mode observer," *J. Aerosp. Eng.*, vol. 28, no. 1, 2015, Art. no. 04014055, doi: 10.1061/(ASCE)AS.19435525.0000331.
[42] K. F. Lu, Y. Q. Xia, and M. Y. Fu, "Controller design for rigid spacecraft attitude tracking with actuator saturation," *Inf. Sci.*, vol. 220, pp. 343–366, Jan. 2013, doi: 10.1016/j.ins.2012.07.039.
[43] Y. G. Li and L. J. Yang, "Neural fuzzy," in *Predictive Control and Its MATLAB Implementation*. Beijing, China: Electronic Industry Press, 2018, pp. 27–30.
[44] J. L. Fernandez-Martinez and E. Garcia-Gonzalo, "Stochastic stability analysis of the linear continuous and discrete PSO models," *IEEE Trans. Evol. Comput.*, vol. 15, no. 3, pp. 405–423, Jun. 2011, doi: 10.1109/TEVC.2010.2053935.
[45] J. Q. Han, *Active Disturbance Rejection Control Technique*. Beijing, China: National Defense Industry Press, 2013, pp. 69–70.
[46] H. Wan and X. H. Qi, "Convergence and stability analysis of linear/nonlinear switching extended state observer," *Inf. Control*, vol. 42, pp. 1758–1764, Sep. 2020, doi: 10.13976./j.cnki.xk.2020.9073.
[47] L. H. Hua, J. F. Zhang, D. J. Li, and X. B. Xi, "Fault-tolerant active disturbance rejection control of plant protection of unmanned aerial vehicles based on a spatio-temporal RBF neural network," *Appl. Sci.*, vol. 11, no. 9, p. 4084, 2021, doi: 10.3390/app110940.84.
[48] H. Wan, X. H. Qi, and J. Li, "Stability analysis of linear/nonlinear switching active disturbance rejection control based MIMO continuous systems," *J. Syst. Eng. Electron.*, vol. 32, no. 4, pp. 956–970, Aug. 2021, doi: 10.23919/JSEE.2021.000082.
[49] J. Li, Y. Xia, X. Qi, and Z. Gao, "On the necessity, scheme, and basis of the linear–Nonlinear switching in active disturbance rejection control," *IEEE Trans. Ind. Electron.*, vol. 64, no. 2, pp. 1425–1435, Feb. 2017, doi: 10.1109/TIE.2016.2611573.
[50] B. Li, Q. Hu, and G. Ma, "Extended state observer based robust attitude control of spacecraft with input saturation," *Aerosp. Sci. Technol.*, vol. 50, pp. 173–182, Mar. 2016, doi: 10.1016/j.ast.2015.12.031.
[51] A.-M. Zhou, K. D. Kumar, Z.-G. Hou, and X. Liu, "Finite-time attitude tracking control for spacecraft using terminal sliding mode and Chebyshev neural network," *IEEE Trans. Syst., Man, Cybern., B (Cybern.)*, vol. 41, no. 4, pp. 950–963, Aug. 2011, doi: 10.1109/TSMCB.2010.2101592.
[52] S. P. Bhat and D. S. Bernstein, "Continuous finite-time stabilization of the translational and rotational double integrators," *IEEE Trans. Autom. Control*, vol. 43, no. 5, pp. 678–682, May 1998, doi: 10.1109/9.668834.
[53] W. Zhang, *Quantitative Process Control Theory*. Boca Raton, FL, USA: CRC Press, 2011, p. 22.
[54] G. Flores, A. Montes de Oca, and A. Flores, "Robust nonlinear control for the fully actuated hexa-rotor: Theory and experiments," *IEEE Control Syst. Lett.*, vol. 7, pp. 277–282, 2023, doi: 10.1109/LCSYS.2022.3188517.

**SHUANG LIANG** was born in 1989. She received the B.Eng. and M.Eng. degrees from Dalian Maritime University, Dalian, China, in 2011 and 2016, respectively. She is currently pursuing the Ph.D. degree with Space Engineering University, Beijing, China. Her research interests include spacecraft orbit dynamics, guidance and control, and space mission analysis.

**YASHENG ZHANG** was born in 1974. She received the B.Eng. and M.Eng. degrees from the National University of Defense Technology (NUDT), China, in 1996 and 1999, respectively, and the Ph.D. degree from Space Engineering University, Beijing, China, in 2006.

She is currently a Professor with Space Engineering University. She has published more than 60 articles and ten monograph publications. Her research interests include spacecraft orbit dynamics, constellation design, guidance and control, and space mission analysis. She received the Young Science and Technology Award of China, the National Science and Technology Progress Award, and the Space Fund Award of China.